MNE 21 (2023) 100228

Contents lists available at ScienceDirect

Micro and Nano Engineering

journal homepage: www.sciencedirect.com/journal/micro-and-nano-engineering

Development of an integrated breath analysis technology for on-chip aerosol capture and molecular analysis

Filip Paeps [a], Thomas Degreef [b], Wout Duthoo [a], Yorick Koumans [b], Erik Emmen [a], Abdulkadir Yurt [a], Elisabeth Marchal [a], Andrey Kossarev [a], Thi-Minh-Tho Dam [a], Rabea Hanifa [a], Joost Van Duppen [a], Zhenxiang Luo [a], Marco Peca [a], Tobe Wauters [b], Wouter Vleugels [b], Nadia Chakrova [b], Johan Berte [b], Floris Vernieuwe [b], Maxime Delgrange [b], Hari Prasanth [b], Sven Van Geyt [b], Frederik Mortier [b], Joren Raymenants [c], Emmanuel André [c], Nik Van den Wijngaert [a], Peter Peumans [a], Tim Stakenborg [a], Bert Verbruggen [a,*]

[a] *Imec, Kapeldreef 75, 3001 Leuven, Belgium*
[b] *Verhaert, Hogenakkerhoekstraat 21, 9150 Kruibeke, Belgium*
[c] *University Hospital Leuven, Herestraat 49, 3000 Leuven, Belgium*

ARTICLE INFO

Keywords:
Breath sampling
Fast qPCR
Silicon impactor
Aerosols
COVID-19
In-vitro diagnosis
Virus detection
Lab-on-a-chip

ABSTRACT

As proven early on in the pandemic, SARS-CoV-2 is mainly transmitted by aerosols. This urged us to develop a silicon impactor that collects the virus particles directly from breath. Performing PCR on these breath samples proved equally sensitive as nasopharyngeal swabs during the first week of an infection [Stakenborg et al., 2022], yet it remained a mostly manual process and PCR turn-around-time was still long. To overcome these drawbacks, we developed a fast and sensitive, fully integrated point-of-need breath test, comprising a novel breath sampler device and PCR instrument. The breath sampler combines virus collection and in-situ RNA amplification. The PCR instrument performs very fast amplification of the released viral RNA. Sample-to-result time was reduced to <20 min with an equal performance as the original manual procedure.

1. Introduction

The SARS-CoV-2 outbreak has resulted in a global pandemic. To help contain the spread, diagnostic platform technologies proved to be indispensable. Nasopharyngeal swabs have been most widely used [1], but are often perceived uncomfortable [2] and remain positive long after contagiousness has subsided. These tests also require a centralized lab and, ideally, a professional to take the sample. Rapid antigen tests have become a popular alternative, allowing for self-testing. Unfortunately, they are less sensitive, especially early in an infection [3]. As a significant fraction of SARS-CoV-2 transmission takes place before symptom onset [4,5], sensitive and early detection is essential, ideally at the point-of-need.

We developed a non-invasive, molecular test to detect SARS-CoV-2 in exhaled aerosols [6]. The device encompasses a silicon impactor to efficiently capture exhaled particles as small as 300 nm, a size assumed small enough to capture the vast majority of all exhaled aerosols potentially containing viruses. In clinical studies, using a simple breathing protocol of about one minute, we demonstrated that our method can detect the onset of an infection at least as early as a nasopharyngeal swab test [3].

While our method is based on the direct molecular detection of SARS-CoV-2, other breath-based tests have been described. Many non-invasive breath tests are based on the detection of volatile organic compounds (VOCs). While clear differences in overall VOC patterns can be observed between infected and non-infected subjects, they suffer from large person-to-person variability, which complicate analyses [7]. Also breath condensates, involving the cooling of exhalates, have been reported as a means for non-invasive testing. The detection rates of these tests have been reported to vary widely [8]. This may at least partially be due to the large dilution of analytes during the collection of breath condensates that are saturated by water vapor. Our method of capturing aerosols directly allows to enrich the sample by collecting respiratory particles of interest in very small volumes, opening a path towards fast,

* Corresponding author.
E-mail address: bert.verbruggen@imec.be (B. Verbruggen).

https://doi.org/10.1016/j.mne.2023.100228
Received 15 December 2022; Received in revised form 14 September 2023; Accepted 23 September 2023
Available online 25 September 2023

miniaturized PCR directly on our impactor [6].

The first clinical tests using our silicon impactor encompassed multiple manual handling steps, leading to long sample-to-result turn-around-time and limiting ease-of-use. For this reason, we here describe a novel breath sampler design and integrated workflow allowing to go from sampling to PCR analysis with minimal manual interventions. This novel breath sampler encompasses an internal mechanism that can be actuated by an in-house developed filling station to bring the captured respiratory particles in contact with PCR and lysis reagents. After filling, the mechanism in the breath sampler can be actuated a second time to seal the impactor for in-situ PCR using an in-house developed qPCR instrument. This allows a fully integrated and rapid workflow. The working principle and pictures of the different developed components are shown in Fig. 1.

2. Material and methods

2.1. General description of the breath sampler design and its manufacturing

The breath sampler (see Fig. 1B) was designed to collect aerosols, bring these in contact with reagents and contain them in a sealed environment while providing an interface for in-situ testing. The core of the breath sampler is the silicon impactor which collects the aerosols. The breath sampler design needed to: 1) allow exhaled breath to flow through the impactor; 2) enable reagents to be brought into contact with the captured aerosols; 3) allow the impactor to be hermetically sealed off during the PCR process. To accommodate this, we placed the silicon impactor (Fig. 2C) on a carrier (Fig. 2B) that could be moved to three different locations, one for each crucial step. We distinguish these as the sampling location, the filling location, and the PCR location.

During design, special attention was given to assure adequate sealing and to prevent the escape of PCR amplicons. The PCR process creates billions of DNA amplicon copies, hence, any amplicon escaping from the breath sampler could have the potential to corrupt future tests in the same room. To cope with this challenge, a pair of PCR lip seals (Fig. 3H) were introduced to press against the impactor carrier from each side when the impactor carrier moves towards the PCR location. Together with the other parts of the sealing stack (Fig. 3), it forms a hermetically enclosed chamber. An additional sealing challenge was for the individual nozzles of the impactor to be closed off to prevent evaporation of liquid reagents during the PCR thermal cycling. To address this, compliant layers covering all nozzles were included to press against both sides of the impactor when the impactor carrier is moved to the PCR location. On top, transparent polydimethylsiloxane (PDMS) (Fig. 3B) was used to allow for the optical subsystem of the PCR instrument to interact with the impactor. On the bottom, thermally conductive Li-2000A tape (Fig. 3D) was used to allow for the most efficient heat exchange between the impactor and the thermal system of the PCR instrument. To prevent the formation of air bubbles between the PDMS and the impactor, which would negatively impact the system's optical performance, the compliant layer is pressed onto the impactor under an angle. This causes air to get pushed out instead of trapped inside.

The breath sampler was developed as a one-time-use disposable product. The housing (Fig. 2H) of the breath sampler was made of two separate polycarbonate shells. Air lip seals (Fig. 2D), made of thermoplastic elastomers (TPE), were over-molded onto the housing. Low-density polyethylene (LDPE) caps (Fig. 2E and J) and transparent foils (Fig. 2G) were added onto the housing to prevent the breath sampler from having apertures during various stages of its use. The impactor carrier was made of brittle polystyrene so that the pulling rods (Fig. 2M), which are part of the carrier, could be easily broken-off. Polystyrene, having a low thermal conductivity, also helped keeping the temperature variations local. The optical and thermal windows (Fig. 3A and G) were

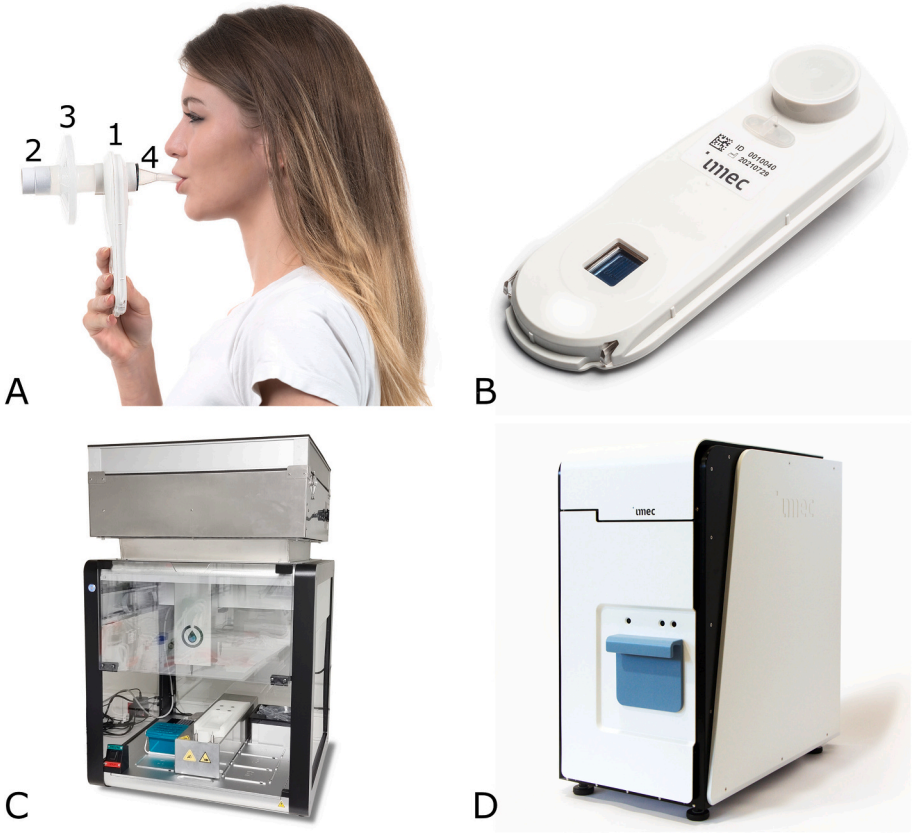

Fig. 1. Overview of the integrated breath sampling hardware. (A) Breath sampler (1) during sampling, connected to a spirometer (2), air filter (3) and mouthpiece (4). (B) Picture of the disposable breath sampler. (C) Picture of the filling station. (D) Picture of the PCR instrument.

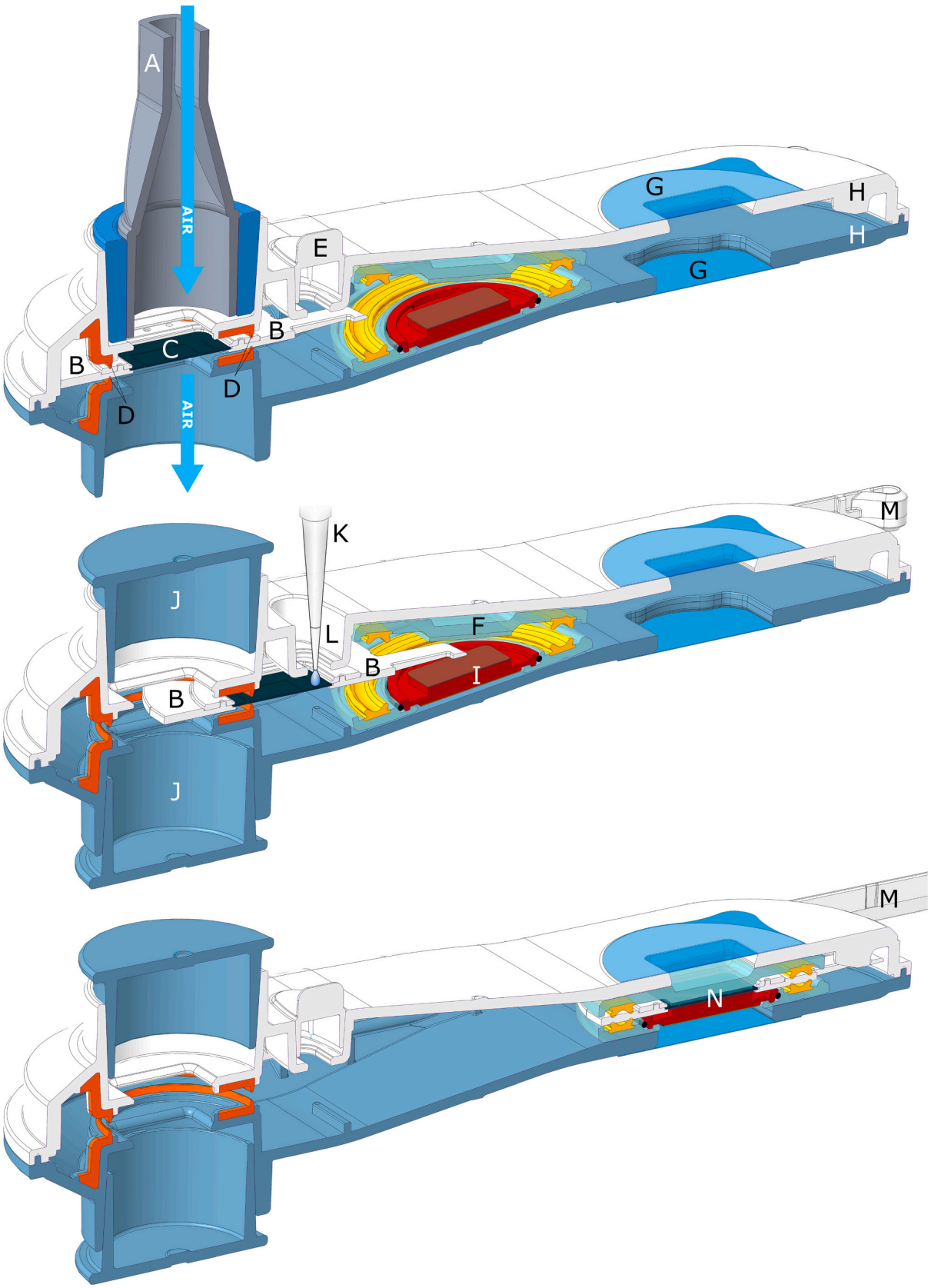

Fig. 2. Cross-section of the breath sampler during sampling (top), while filling (middle) and when sealed before PCR (bottom). The key components are indicated: (A) Mouthpiece; (B) Impactor carrier with (M) pulling rods; (C) Silicon impactor; (D) Air lip seals; (E) Cap on the filling port; (F) Optical interface; (G) Transparent foils; (H) Housing shells; (I) Thermal interface; (J) Caps on the sampling ports; (K) Pipette tip; (L) Filling port; (N) Sealing stack.

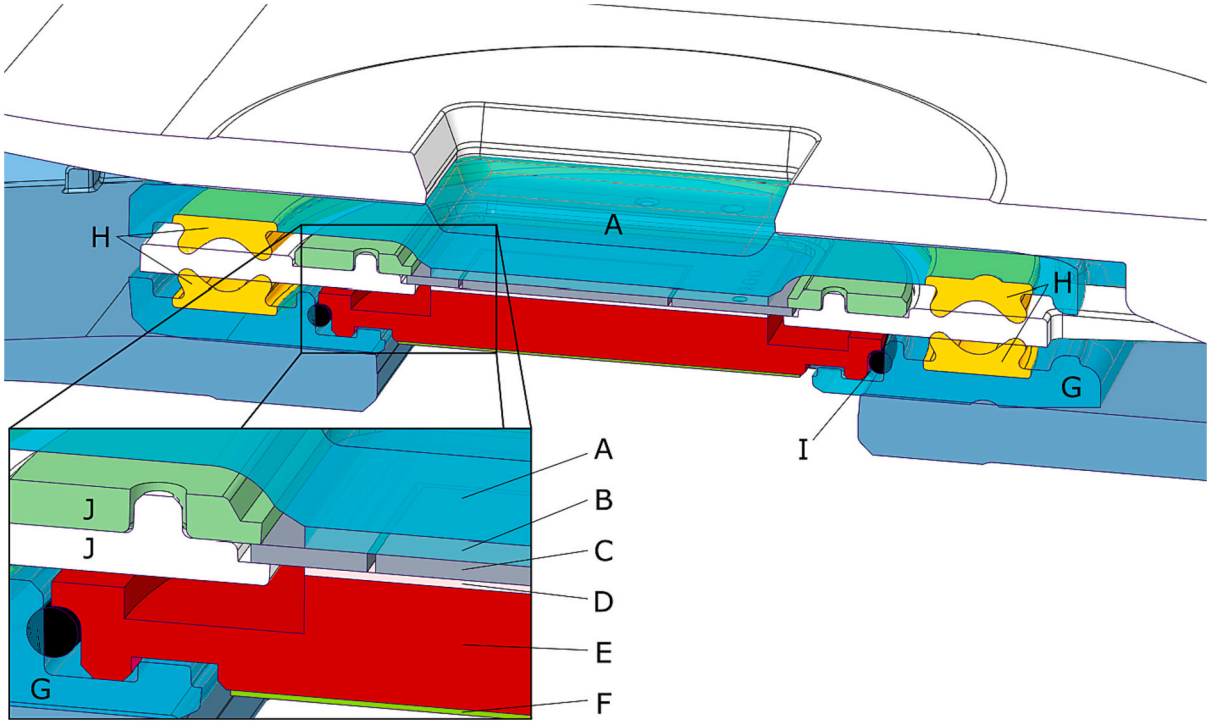

Fig. 3. Close-up of the sealing stack (i.e., breath sampler during PCR location). Optical interface consisting of (A) COP optical window and (B) PDMS optical compliant layer. (C) Silicon impactor. Thermal interface consisting of (D) Li-2000A thermal compliant layer, (E) aluminum thermal plate, (F) graphite layer and (G) COP thermal window. (H) TPE PCR lip seals. (I) EPDM rubber ring. (J) Polystyrene impactor carrier.

made of cyclic olefin polymers (COP) to assure good optical performance. The TPE PCR lip seals (Fig. 3H), introduced to prevent amplicon escape, were over-molded onto the COP parts. All these plastic parts were injection molded. All components were assembled in an ISO 7 clean room. For the optical interface, a PDMS optical compliant layer was treated with plasma and added by hand. For the thermal interface, a machined aluminum plate (Fig. 3E) was covered with two thermally conductive layers: Li-2000A on top and graphite (Fig. 3F) on the bottom to assure good thermal connection of the impactor to the PCR instrument. The aluminum plate was then press-fitted into the COP thermal interface with an ethylene propylene diene monomer (EPDM) rubber ring (Fig. 3I) in between. The two shells of the housing were ultrasonically welded together. A label with a unique, traceable serial number and a corresponding barcode was added to finish the assembly. Each breath sampler was packaged individually in a plastic bag and a cardboard box.

2.2. Functional steps of the breath sampler during operation

A schematic animation of the process explained in the following chapters is available as Supplementary Video 1.

2.2.1. Collecting aerosols

The breath samplers were stored at room temperature but were heated up in an oven to 60 °C before use to prevent condensation of aerosols onto its internal parts during sampling. Before sampling, the caps which cover the air inlet and outlet ports were removed. A medical grade mouthpiece (Respitek PV-28BG) was connected to the air inlet and an air filter (Piston Medical PBF-100-G-C) followed by a spirometer (Mir Minispir) to the outlet. During sampling (Fig. 1A), the breath exhaled by the sampled individual was forced to flow through the impactor. This impactor was fabricated as a monolithic silicon chip with 1600 air inlet and 1144 outlet nozzles in between which the air is forced to follow an S-shaped duct. As such, the exhaled aerosols were captured using inertial impaction as described before [6]. Air flow was prevented to enter the rest of the enclosure by the air lip seals (Fig. 2D) around the impactor carrier (Fig. 2B). The air filter behind the breath sampler (not depicted) was included as an extra safety measure, avoiding virus particles to enter the sampling area. The spirometer was used to guide test-takers through the breathing protocol by giving feedback on their progress and the desired flow rate (set at 0.3 L/s), as well as to collect additional data on flow rate and total sampling volume. The total sampling time, including eight inhalation and exhalation steps, was typically about one minute. After sampling, the mouthpiece, air filter and spirometer were disconnected from the breath sampler and the air inlet and outlet ports were recapped.

2.2.2. Filling with reagents

To add the necessary reagents to the breath sampler for testing, a commercial pipetting robot (Opentrons OT-2) was altered to function as a filling station (see Fig. 1C). To move the breath sampler's impactor carrier to different positions, pulling rods (Fig. 2M) -which are part of the carrier (Fig. 2B)- were actuated by the filling station. To achieve this, a dedicated holder for the breath sampler including a linear actuator was integrated as part of the filling station. During use, the breath sampler was placed into the holder after its filling port was uncapped. The pulling rods were hereby brought in contact with two pins connected to the linear actuator. The impactor carrier was pulled for a first time to bring the impactor to the filling location. In this location, the filling inlets of the silicon impactor were exposed and 44 µL of reagents were dispensed on top by the filling station's robotic pipetting system. Besides for detection of SARS-CoV-2, the reagents also allowed for an internal control based on FIPV (Feline Infectious Peritonitis Virus). The full contents of the reagents are described in Supplementary Table B. Filling of the impactor happened automatically by capillary actuation. After filling, the pipette tip was retracted and disposed in a waste bag.

2.2.3. Sealing

After filling, the impactor carrier was pulled in between the optical and thermal interfaces (Fig. 2F and I) by the linear actuator. During this

pulling movement, both interfaces were pulled along. The interfaces were forced to move slowly under an angle towards the impactor by the shape of the housing. The goal is to prevent air bubbles from getting in between the interfaces and the impactor and to assure that any reagent left on top of the impactor spreads evenly. When reaching the end position, the PCR lip seals of the optical and thermal interfaces were pressed by the exoskeleton housing against the impactor carrier, as shown in detail on Fig. 3.

The breath sampler was removed from the filling station and the pulling rods were snapped off from the impactor carrier so that they were out of the way during further handling. Also, the transparent foils (Fig. 2G) were removed to expose the optical and thermal interfaces of the breath sampler. The entire process of filling and sealing was always finished in about two minutes after which the breath sampler was ready to be inserted into the PCR instrument.

2.3. PCR instrument

The PCR instrument (see Fig. 1D) consists of two main subsystems: an optical subsystem and a thermal subsystem. During operation, both subsystems are controlled by the embedded hardware components including a main controller, a USB hub to transfer data to the external computer and a series of additional electronic boards for handling sensors, specific actuators, LEDs etc. All subsystems have been integrated into a single housing.

2.3.1. Optical subsystem

The optical subsystem was made to operate in an epi-illumination mode. In the illumination path, two laser beams originating in the laser box (Fig. 4D) were coupled into a fiber and despeckled by applying vibrations to the fiber. The two beams were selected to detect both the potential presence of SARS-CoV-2 viral RNA ($\lambda = 488$ nm) as well as an internal control ($\lambda = 532$ nm). Despeckled laser beams, passing through the beam expanding optics (Fig. 4C), were carefully chosen to achieve uniform illumination over the sample area of 12 × 12 mm. The laser beams were directed towards the silicon impactor (Fig. 4I) by a dichroic mirror (Fig. 4G). During testing, the fluorescent light generated during in-situ amplification was split into two identical channels by dichroic mirrors, such that the sample fluorescence and control fluorescence were captured on separate cameras (Fig. 4A and B). Images of both detection channels were captured with a magnification close to 1× which allowed inspection of individual wells over the complete sample field of view. The bill-of-materials of this subsystem can be found back in Supplementary Table A.

2.3.2. Thermal subsystem

The thermal subsystem (Fig. 4J) was designed to rapidly heat and cool the breath sampler's thermal interface. A thermoelectric cooler (TEC-Microsystems 1MA10–127-03), of which the cold side was conductively cooled by a liquid coolant loop to maximize cooling rates, was used as the core of the thermal subsystem. To assure proper thermal contact between the TEC and the breath sampler, the TEC was placed on a self-centering pushing module. Accurate control of the PCR reagent temperature required an accurate measurement. This was not possible in a direct way due to the lack of an on-silicon temperature measurement. Instead, a temperature sensor was integrated in the top surface of the TEC and the measurement results were correlated to the impactor temperature based on a gray box model.

To create this model, a lumped body model of the thermal stack was created in Simulink and converted into a MIMO (multiple input multiple output) state space representation with symbolic thermal model parameters (conductivity and thermal mass). Temperature data of impactor and TEC were measured for multiple systems and conditions, to gather a representative training dataset. The real-world TEC data was used as an input for the thermal model, and the output data of the model (modeled impactor temperature) was compared to the real-world

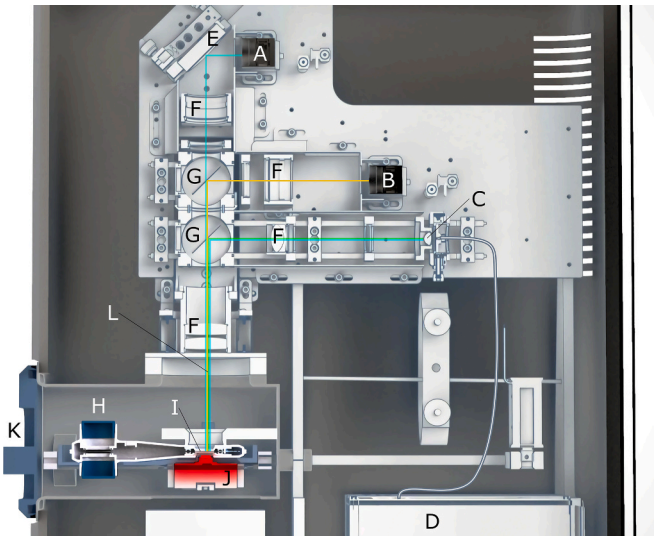

Fig. 4. Schematic of the inside of the PCR instrument. (A) Green channel camera; (B) Blue channel camera; (C) Laser emitter, driven by an optical fiber connected to the (D) laser box; (E) Mirror; (F) Lenses; (G) Dichroic mirrors; (H) Breath sampler with (I) silicon impactor; (J) Thermal subsystem; (K) Breath sampler insertion port; (L) Light beams. (For interpretation of the references to colour in this figure legend, the reader is referred to the web version of this article.)

impactor data, measured locally on the impactor surface of modified breath samplers that integrated additional temperature sensors. The model parameters were tuned to find a best fit between modeled and real-world impactor temperature. The optimized model was validated by a simulation with a validation data set and real-world testing.

The performance of the thermal system was dependent on the thermal model accuracy, the variation of thermal characteristics of the breath sampler, the proper tuning of control parameters, as well as (to lesser extent) the protocol itself. Based on the verification test results and additional data that were analyzed over the course of development, we were able to define a set of thermal model and control system parameters that ensured thermal performance regardless of the breath sampler or the protocol that was used.

2.3.3. Performing PCR

To perform a qPCR analysis, the breath sampler was inserted into the instrument and the port (Fig. 4K) was closed by the user. After automatic detection of the breath sampler and its unique identification code, the port was locked and the thermal pusher was engaged. An initial set of images was displayed, allowing the user to confirm proper quality of the silicon impactor, after which the processing was started. From this moment onwards, a user-defined protocol (see below) was followed setting the temperatures, timings, and moments for camera activation.

The protocol used during the clinical test assured lysis and reverse transcription for 2 min at 50 °C. Next, the temperature was raised to 95 °C during 20 s for inactivation of the reverse transcriptase and the initial denaturation. This was followed by a series of 45 thermal PCR cycles (8 s at 66 °C for annealing, extension and acquiring fluorescent images from both channels, followed by a ramp to 92 °C for denaturation). After cycling, a cooldown step was included to ensure the breath sampler was at a safe temperature to touch when it was removed from the system. The contents of the reagents are described in Supplementary Table B.

2.3.4. Image processing

At the end of the process, pre-processed images and raw data were automatically uploaded to an in-house developed cloud system by which further image processing was performed through curve fitting. The

qPCR data was obtained by extracting the mean fluorescence intensity in each nozzle for each cycle and normalizing it to a range from 0 to 1. The Ct values were calculated using sigmoidal fitting of the qPCR data as described before [9]. In case no fluorescence was detected, no Ct value was generated, and the sample was labeled as negative. As can be seen on Fig. 5, a Ct value was generated for each nozzle on the impactor. From this, an overall Ct value was automatically derived.

2.4. Sealing tests

Hermetic sealing of the impactor was required to prevent the escape of virus particles and PCR amplicons. To verify that this requirement was met, the sealed chamber of a modified breath sampler was pressurized to 700 mbar above environmental pressure. Then, the pressure was monitored for 5 min to verify if there was any pressure loss.

As a second test, three breath samplers were filled with Chinese Hamster Ovary (CHO) genomic DNA at a concentration of 3 ng/μL. The breath samplers were put in the PCR instrument and the PCR protocol was run. Before and after the run, swipes were taken from various locations on the breath samplers. The breath samplers were also cut open while keeping the sealing stack closed and surface swabs were taken around the sealing rims. All the swabs were tested in the LightCycler® 480 System (Roche Diagnostics) using the resDNASEQ™ Quantitative CHO DNA kit (Applied Biosystems) to test for the presence of CHO gDNA. The default PCR cycling conditions were maintained as per the manufacturer's instructions: Initial denaturation at 95 °C for 10 min, followed by 40 cycles of denaturation for 15 s at 95 °C and annealing/extension for 1 min at 60 °C. A standard dilution series of CHO gDNA and negative controls were included in each run.

As a third check, swabs were taken again on various locations of the breath sampler but using SARS-CoV-2 synthetic gRNA as template. The same PCR cycling conditions were used as in clinical testing (see section 2.7). This third check was testing for amplicon release during PCR.

2.5. Thermal tests

One of the challenges in the system design was to allow for a fast and accurate PCR, meaning reverse transcription and quantitative PCR combined to happen in <15 min. For the PCR to function optimally, the temperature deviations requirements were limited to ±0.5 °C at 66 °C and ± 2 °C at 92 °C. Temporal (1 s) overshoots were allowed of 1 °C at 66 °C up to 4.5 °C at 92 °C.

To evaluate the thermal performance, three breath samplers were equipped with two thermocouples in between the PDMS optical compliant layer and the silicon impactor. The same thermal protocol as used during the clinical test was run and the actual temperature on the impactor was monitored. The thermal steps together with key parameters including ramp up-time, cooldown time and temperature accuracy were automatically analyzed by means of a python script for the complete data set.

2.6. Optical tests

The optical subsystem was designed from scratch, requiring a thorough verification. To test spatial homogeneity of the system, uniformly fluorescent slides were introduced into the PCR instrument and images were acquired from each channel. The uniformity was calculated on these images using ImageJ. The optical subsystem of each PCR instrument was calibrated by performing a flatfield correction on a Macbeth 40% gray pad. The spatial homogeneity was tested twice: once with the flat field correction disabled and once with the correction enabled.

Temporal stability during thermal cycling was tested by running a PCR test on a breath sampler filled with reagents, but without presence of viral DNA to ensure a constant fluorescence.

2.7. Clinical tests

To demonstrate a proof-of-concept for this newly developed system, a clinical study was set up in which the integrated workflow with in-situ PCR as described above was compared to a non-integrated workflow in which PCR was performed off-chip (similar as described in full detail before [1]).

A total of 40 vaccinated SARS-CoV-2 positive subjects, as determined by nasopharyngeal swab PCR, were invited to take part in this study. After giving their informed consent, subjects underwent two additional nasopharyngeal swabs (one for PCR, another for a rapid antigen test). Standard flocked cotton swabs were used for the nasopharyngeal samples. They were collected in 1.5 mL zymo-medium (Zymo Research). Abbot Panbio™ COVID-19 Ag Rapid Test Devices were used for the point-of-care antigen test.

For the breath tests, half of the devices were assigned to the non-integrated workflow, the other half to the integrated workflow. The order in which these samples were taken was counterbalanced across subjects. Samples were thus taken in duplicate. The positive Ct values were retained. If both were positive, the Ct values were averaged. Breath samples were collected by letting the subjects exhale eight times through

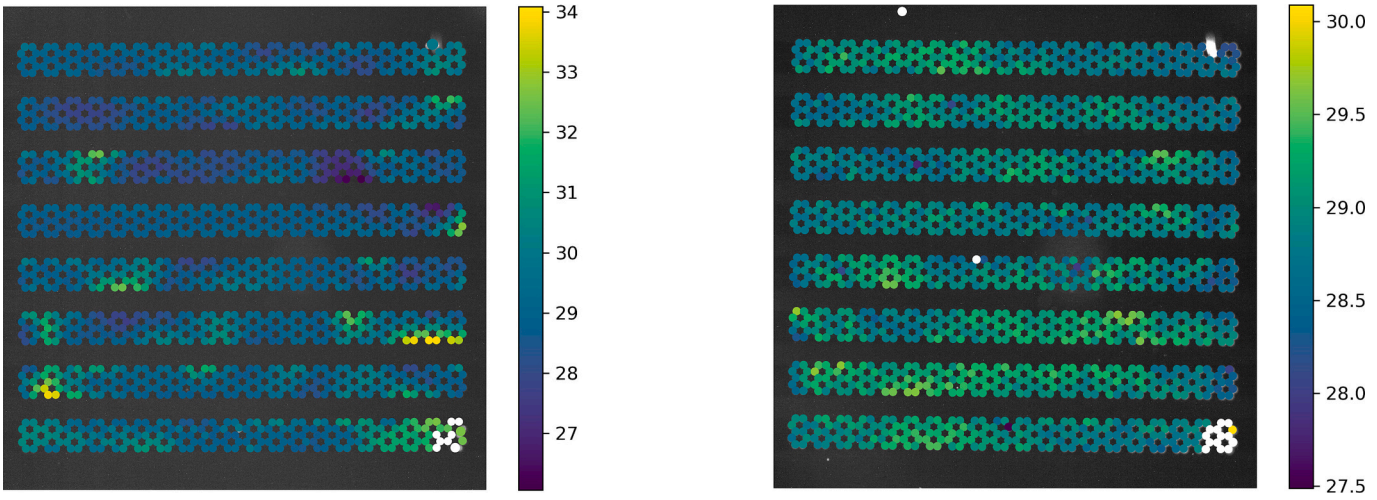

Fig. 5. The image processing script generates a Ct value for each detected nozzle on the silicon impactor. Left: blue channel indicating the presence of SARS-CoV-2. Right: green channel (internal control). As the blue channel has an overall Ct value of 29.2, the subject of this sample was exhaling the SARS-CoV-2 virus. (For interpretation of the references to colour in this figure legend, the reader is referred to the web version of this article.)

the breath samplers while vocalizing (producing the sound "u") for 4 s. In between two exhalations, subjects could inhale via the nose or away from the device. Total sampling time amounted to 64 s. Target flow rate of the feedback software was set at 0.3 L/s, as established during prior protocol optimization in our lab. Total volume of air collected after 8 times 4 s thus amounted to 9.6 L on average. Subjects were instructed not to go beyond their comfort zone and could stop at any moment.

3. Results

3.1. Sealing test results

Eight breath samplers had their sealed chambers pressurized for testing. On average, a pressure drop of 6.5 mbar was observed with a maximum of 18.7 mbar. This amount was found to be acceptable to initiate the CHO tests.

No release of CHO gDNA was observed for any of the surface swabs taken from the breath samplers filled with a high concentration of CHO DNA, indicating no release of gDNA during thermal cycling. Also no amplicon release was observed during control runs of the SARS-CoV2 N2 assay testing on the breath sampler using SARS-CoV2 gRNA as template prior to clinical testing.

3.2. Thermal test results

During the initial phase of the protocol, lysis and reverse transcription were maintained within a tolerance of 50 °C ± 0.5 °C and inactivation at 95 °C was maintained within a tolerance of ±2 °C. Throughout cycling, heating ramp rates of 14.9 °C/s were noted, rapidly heating the impactor to 92 °C ± 2 °C. Rapid cooling was observed at rates of −6.2 °C/s to bring the temperature to a stable 66 °C ± 0.5 °C (see Fig. 6). An average cycle took 16 s which successfully led to a total processing time of <15 min.

3.3. Optical test results

Using ImageJ, we determined the following spatial uniformity data. Without flatfield correction, 88% and 97% of the fields of view of the blue and green channel, respectively, were at least 70% homogeneous. After the flatfield correction was applied, the non-uniform field was corrected within 5% error margin of the flat-fielding (see Fig. 7).

During the temporal stability test, air bubbles got trapped during filling, which caused only 94% of the holes to be filled correctly. The correctly filled holes on the test chip showed consistent fluorescent intensity during the test run of 45 cycles. The relative temporal fluctuation of the intensity (measured as 1σ from the mean value) is found to be lower than 0.05 for the filled holes.

3.4. Clinical test results

The main objective of this study was to demonstrate proof-of-concept for the newly developed system by comparing the integrated workflow with in-situ PCR to a non-integrated workflow in which PCR was performed off-chip, not to establish the clinical performance of the device. Results indicated a very similar performance, yielding a significant correlation of the Ct values for the integrated and non-integrated workflows ($R = 0.87$, $p < 0.001$; see Fig. 8A).

Moreover, Ct values of two consecutive test runs showed a similarly high correlation for the integrated workflow ($R = 0.83$, $p < 0.001$) and the non-integrated workflow ($R = 0.78$, $p < 0.001$) (see Fig. 8B).

4. Discussion and conclusion

In this paper, we described the development of an innovative, integrated breath sampler. We combined multiple primary functions in a single disposable: aerosol collection, reagent addition and sealing the PCR cavity. After optimizing aerosol collection earlier [3,6], we successfully solved the remaining challenge of hermetic sealing in combination with a good thermal resistance path. In parallel, we developed a custom PCR instrument, with optical and thermal capabilities to perform a complete assay in 15 min. Finally, the complete system was used in a clinical setting, where we demonstrated both the fast time to result and a sensitivity on par with our results generated with a manual workflow [6].

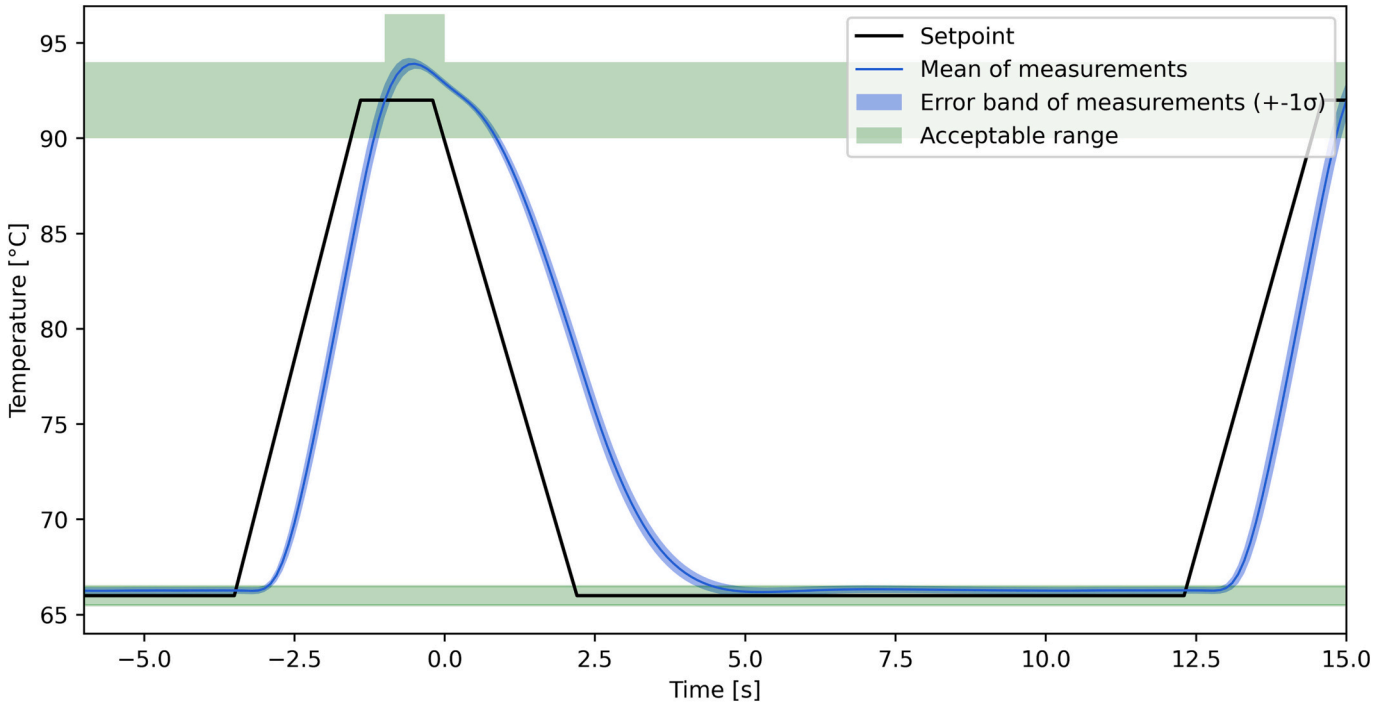

Fig. 6. Comparison between setpoint and measured values during thermal cycling. The graph shows the mean and standard deviations measured over all 45 cycles of the three breath samplers.

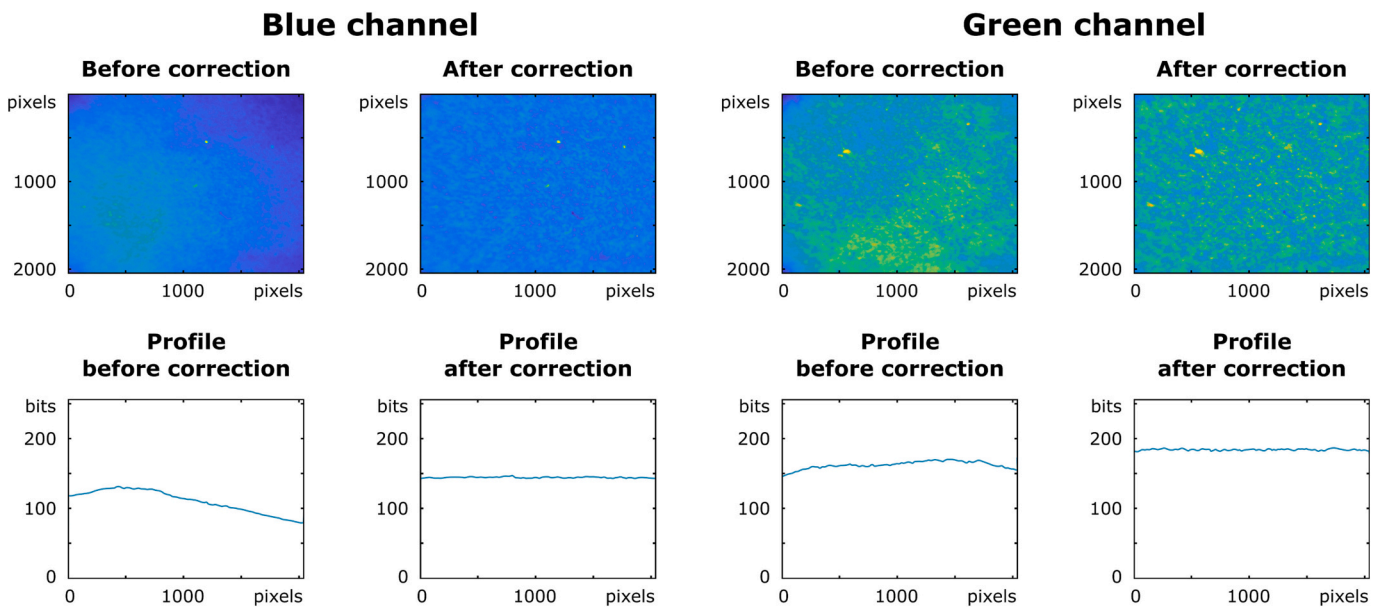

Fig. 7. Pseudo-colored images before and after correction for both channels. The profiles indicate the intensity values measured on the center line.

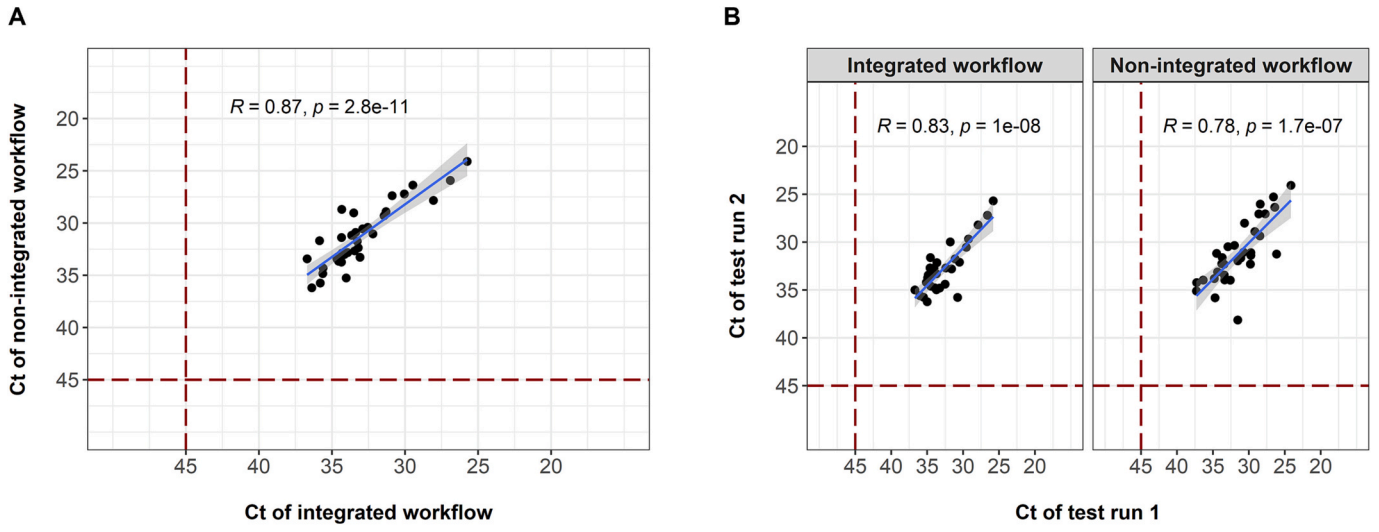

Fig. 8. (A) Correlation of the Ct values obtained from the non-integrated workflow and the Ct values of the integrated workflow. (B) Correlation between Ct values of the first and second run, plotted separately for the integrated and non-integrated workflow.

We believe the described breath sampling system is the first step towards a true point of care diagnostic solution for a range of applications. We already achieved good results for clinical performance, speed, robustness, and integration, but compared to other point of care PCR solutions [9], additional efforts are required to simplify the workflow and to reduce the footprint and cost of both instrument and disposable.

On the disposable, significant cost and size reduction could be achieve if we reduce the size of the silicon impactor chip. This can be achieved by packing the holes closer together and reducing the non-functional silicon area. On the instrument, the complexity, size and cost of the optical module could be significantly reduced by moving to LED illumination and a single detector. Additionally, the workflow could be simplified by adding the reagent additional functionality to the PCR instrument, removing the extra pipetting robot completely.

Besides reduction of complexity and cost, we can still improve the time to result from 15 min down to 5 min [10] if we can further optimize the assay and reduce the thermal resistance between the thermal module and the impactor. A TEC could be built into the silicon impactor chip itself along with temperature control. This could reduce the time required for the PCR process even further while again simplifying the PCR instrument as it would not need a heating module anymore. Another benefit of this approach could be the ability to slightly heat the chip before or during sampling to prevent condensation, avoiding the need to preheat the breath samplers.

In conclusion, we have developed a novel, truly convenient exhaled breath-based test that matches the state-of-the-art with regards to diagnostic accuracy. Our new system combines efficient aerosol capturing and reproducible PCR quantification, demonstrated via clinical tests. As such, it combines the non-invasive and comfortable sampling of other VOC based breath tests with the speed of rapid antigen tests and sensitivity of nasal swab-based PCR methods. This integrated approach opens the door towards point-of-care applications in which no manual lab work is required. Furthermore, the PCR turn-around time was significantly decreased, enabling the technology to be used for applications that require relatively fast results. Our technology has the potential to compete with current standard molecular tests and may

continue to provide exciting new insights into the heterogeneity and dynamics of exhaled viral load shedding. While the COVID-19 pandemic acted as a catalyst for this development, we are now also pursuing other applications.

Supplementary data to this article can be found online at https://doi.org/10.1016/j.mne.2023.100228.

Declaration of Competing Interest

The authors declare that they have no known competing financial interests or personal relationships that could have appeared to influence the work reported in this paper.

Data availability

Data will be made available on request.

References

[1] R.A. Lee, J.C. Herigon, A. Benedetti, N.R. Pollock, C.M. Denkinger, G. Scholar, Performance of saliva, oropharyngeal swabs, and nasal swabs, J. Clin. Microbiol. 59 (2021) e02881–20.

[2] N.N. Kinloch, A. Shahid, G. Ritchie, W. Dong, T. Lawson, J.S.G. Montaner, M. G. Romney, A. Stefanovic, N. Matic, C.J. Brumme, C.F. Lowe, Z.L. Brumme, V. Leung, Evaluation of nasopharyngeal swab collection techniques for nucleic acid recovery and participant experience: recommendations for COVID-19 diagnostics, Open Forum Infect. Dis. 7 (2020) 1–6, https://doi.org/10.1093/ofid/ofaa488.

[3] J. Raymenants, W. Duthoo, T. Stakenborg, B. Verbruggen, J. Verplanken, J. Feys, J. Van Duppen, R. Hanifa, E. Marchal, A. Lambrechts, P. Maes, E. André, N. Van den Wijngaert, P. Peumans, Exhaled breath SARS-CoV-2 shedding patterns across variants of concern, Int. J. Infect. Dis. (2022), https://doi.org/10.1016/j.ijid.2022.07.069.

[4] E.A. Meyerowitz, A. Richterman, R.T. Gandhi, P.E. Sax, Transmission of sars-cov-2: a review of viral, host, and environmental factors, Ann. Intern. Med. 174 (2021) 69–79, https://doi.org/10.7326/M20-5008.

[5] X. He, E.H.Y. Lau, P. Wu, X. Deng, J. Wang, X. Hao, Y.C. Lau, J.Y. Wong, Y. Guan, X. Tan, X. Mo, Y. Chen, B. Liao, W. Chen, F. Hu, Q. Zhang, M. Zhong, Y. Wu, L. Zhao, F. Zhang, B.J. Cowling, F. Li, G.M. Leung, Temporal dynamics in viral shedding and transmissibility of COVID-19, Nat. Med. 26 (2020) 672–675, https://doi.org/10.1038/s41591-020-0869-5.

[6] T. Stakenborg, J. Raymenants, A. Taher, E. Marchal, B. Verbruggen, S. Roth, B. Jones, A. Yurt, W. Duthoo, K. Bombeke, M. Fauvart, J. Verplanken, R. S. Wiederkehr, A. Humbert, C. Dang, E. Vlassaks, A.L. Jáuregui Uribe, Z. Luo, C. Liu, K. Zinoviev, R. Labie, A.D. Frederiks, J. Saldien, K. Covens, P. Berden, B. Schreurs, J. Van Duppen, R. Hanifa, M. Beuscart, V. Pham, E. Emmen, A. Dewagtere, Z. Lin, M. Peca, Y. El Jerrari, C. Nawghane, C. Arnett, A. Lambrechts, P. Deshpande, K. Lagrou, P. De Munter, E. André, N. Van den Wijngaert, P. Peumans, Molecular detection of SARS-COV-2 in exhaled breath at the point-of-need, Biosens. Bioelectron. 217 (2022), https://doi.org/10.1016/j.bios.2022.114663.

[7] M. Phillips, J. Herrera, S. Krishnan, M. Zain, J. Greenberg, R.N. Cataneo, Variation in volatile organic compounds in the breath of normal humans, J. Chromatogr. B Biomed. Sci. Appl. 729 (1999) 75–88, https://doi.org/10.1016/s0378-4347(99)00127-9.

[8] E. Nwanochie, J.C. Linnes, Review of non-invasive detection of SARS-CoV-2 and other respiratory pathogens in exhaled breath condensate, J. Breath Res 16 (2022), https://doi.org/10.1088/1752-7163/ac59c7.

[9] V. Garzarelli, M.S. Chiriacò, M. Cereda, I. Autuori, F. Ferrara, Miniaturized real-time PCR systems for SARS-CoV-2 detection at the point-of-care, Clin. Chim. Acta 536 (2022) 104–111, https://doi.org/10.1016/j.cca.2022.09.014.

[10] Q. Cai, M. Fauvart, R.S. Wiederkehr, B. Jones, P. Cools, P. Goos, M. Vaneechoutte, T. Stakenborg, Ultra-fast, sensitive and quantitative on-chip detection of group B streptococci in clinical samples, Talanta. 192 (2019) 220–225, https://doi.org/10.1016/j.talanta.2018.09.041.